C. R. Physique 17 (2016) 874–892

Contents lists available at ScienceDirect

Comptes Rendus Physique

www.sciencedirect.com

Polariton physics/Physique des polaritons

# Polariton interactions in semiconductor microcavities

## *Interactions entre polaritons dans des microcavités semiconductrices*

Benoit Deveaud

*EPFL, Physics Institute, CH-1015 Lausanne, Switzerland*

ARTICLE INFO

*Article history:*
Available online 3 June 2016

*Keywords:*
Exciton
Polariton
Microcavity
Spectroscopy
Semiconductor
Interaction

*Mots-clés :*
Exciton
Polariton
Microcavité
Spectroscopie
Semiconducteur
Interaction

ABSTRACT

In this review, we will try to summarize the results that we have obtained on the measurement of polariton interactions. We will describe here the samples, the experimental systems and some of the important results. We will also give a few highlights on the theoretical description of these results. One of the main topics of this review will be the observation of the Feshbach resonance for polaritons, and its interpretation through the coupling of two lower polaritons into a biexciton.



RÉSUMÉ

Dans cet article de synthèse, nous nous efforcerons de présenter les résultats qui ont été obtenus en matière d'interactions entre polaritons. Nous décrirons les échantillons, les systèmes expérimentaux et certains résultats importants. Nous donnerons aussi quelques éclaircissements quant à la description théorique de ces résultats. Un des principaux sujets qui seront abordés ici est l'observation de la résonance de Feshbach pour les polaritons et son interprétation à travers le couplage de deux polaritons bas vers un biexciton.



## 1. Introduction

Exciton polaritons in a semiconductor microcavity constitute a very interesting and unique quasiparticle system where excitons confined in a semiconductor quantum well are strongly coupled with photons confined in the microcavity [1]. Such quasiparticles show properties that originate from this double origin.

First, from both constituents, they show a bosonic character. From their photon part, the polaritons inherit a very small mass (more than 4 orders of magnitude less than the electron mass) as well as a very short lifetime (mainly limited by the $Q$-factor of the microcavity). From their excitonic component, the polaritons acquire the ability to interact. From both constituents, the polaritons also carry a spin that is shared by the exciton and the photon part of the polariton.

*E-mail address:* benoit.deveaud@epfl.ch.

http://dx.doi.org/10.1016/j.crhy.2016.05.004
1631-0705/

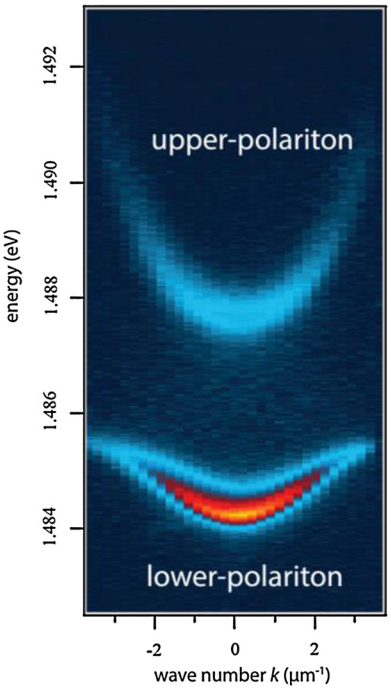


**Fig. 1.** Far-field emission from a planar semiconductor microcavity.

Such properties are reflected by a number of properties that do not need to be described in great detail here (see for example the following reviews on such topic [2–4]). We will simply highlight here some of them. From their bosonic character and very small mass, they are able to condense at rather high temperatures [5,6], even up to room temperature [7–9]. From their interactions, polaritons can form a quantum fluid where superfluid properties have been evidenced [10, 11] together with quantized vortices and dark solitons [12–15]. In such fluids, the existence of the Bogoliubov ghost branch has been demonstrated through heterodyne four-wave mixing experiments [16,17]. The polaritons also evidence interesting bistable properties allowed by the interactions of their excitonic constituents [18,19]. The possible use of such bistable properties has been considered for many very interesting devices [20,21]. Finally, the spin properties of both components of the polariton bring a wide range of very interesting properties, with in particular the existence of half vortices [22,23] and the observation of the spin–Hall effect [24,25]. At the same time, the spin introduces additional degrees of freedom in our system with the possibility of a Feshbach resonance [26,27] and the existence of multistability [28,29].

In the present review paper, we will describe the results of our measurements on the interactions between polaritons and the influence of these interactions on the observed properties of excitonic polaritons. In order to be able to assess the polariton fluid more precisely, we decided to report on resonant experiments where the fluid is in fact not acquiring its coherence spontaneously. This of course does not mean that the interactions that occur under non-resonant excitation schemes, and in particular the interactions with the exciton reservoir, are not of importance. This paper is organized in the following way. In a first part, we will give some details on the samples that have been used and on their growth and preparation. In a second part, we will describe some of the specificities of the experiments that have been performed. Then, we will move to bistability and multistability followed by the detailed study of the interaction between polaritons and, in particular, the case of a Feshbach resonance. In the last part of this review, we will present the connection between our measurements and the measurement performed in the lower polariton basis.

## 2. Samples and experiments

Microcavities have been prepared with many different semiconductor systems. In fact, the work on microcavity excitonic polaritons evolved from the work on VCSELs (Vertical Cavity Surface Emitting Lasers) [30,31] that allowed optimizing the growth of monolithic DBR mirrors, an essential ingredient for preparing microcavities. The first observation of a microcavity polariton was indeed realized in a structure that was meant to be a VCSEL [1].

Similar structures have then been used to observe microcavity polaritons, starting with the same material system, i.e. GaAs-based cavities [32,33]. One of the best ways to measure in details the characteristics of the structure is to realize a far-field image [34] such as the one shown in Fig. 1, as this allows one to assess precisely the coupling strength and the detuning characteristics of the system.

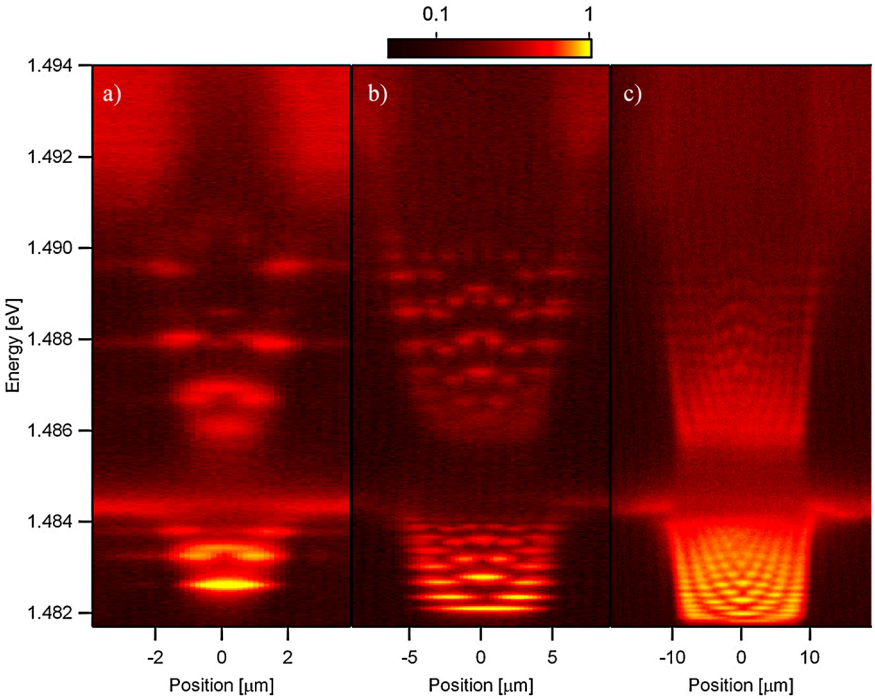


**Fig. 2.** Spatially resolved photo-luminescence of polaritons confined in cylindrical mesas of different sizes: (a) ≈3 μm, (b) ≈10 μm, and (c) ≈20 μm. The PL intensity is plotted in a normalized log color scale. Confined lower polariton states are visible below 1.484 eV. Confined upper polariton states are found between 1.485 eV and 1.490 eV. The two-dimensional excitonic-like lower-polariton energy is 1.4845 eV, and the two-dimensional photonic-like upper polariton energy is visible above 1.492 eV (from the PhD thesis of Gaël Nardin [43]).

Microcavities are now prepared in a very wide variety of materials, from standard semiconductors to more "exotic" systems such as organic materials. In many cases now, the mirrors are not any more monolithic, but could be realized for example from dielectric mirrors or even using external mirrors or a fiber-based cavity [35,36].

Our own samples have been realized in the GaAs system using as quantum wells not the more standard GaAs quantum wells, but InGaAs quantum wells with low indium content. This comes with some difficulties such as the strain in the quantum wells, which may eventually be transferred into strain in the mirrors [37], but comes also with the great advantage that the experiments can be realized in transmission mode, which allows obtaining a much higher signal to noise ratio thanks to the suppression of the back-reflected light from the excitation laser. Let us note here that, in InGaAs-based cavities, spontaneous condensation is very difficult to observe also because of the coupling between the different quantum wells due to their very shallow depth [38]. Getting quantum wells with a larger indium content is therefore a necessity to obtain condensation [39], which comes at the expense of the quality of the quantum wells, and therefore of their linewidth.

In order to be able to manipulate more precisely the polaritons, it is of major importance to be able to confine them. This has been understood quite early and this has led to different possible techniques, of which each one displays advantages and drawbacks. A simple technique consists in depositing a patterned metallic layer on top of the last layer of the DBR mirror. This changes the confinement energy of polaritons and therefore allows their manipulation, although the potential change is very small [40]. Another technique has been first proposed at the University of Wurzburg (Germany) [41], and is now routinely used in many places, in particular at the LPN in Marcoussis (France) [42]. It consists in etching the whole of the thickness of the microcavity, allowing one to provide a deep photonic confinement.

Our own technique aims at being able to realize confinement of polaritons allowed us to realize very high quality mesas of any shape, as evidenced by Fig. 2. The principle has been given in details in [44,45] and consists of the following trick. We grow the first half of the cavity, including the spacer with the quantum wells. Then we use microtechnology to etch the desired structures by something like 5 nm. This will provide confinement for photons and then for polaritons.

As far as the experiments are concerned, most of them are now rather standard. Two of them nevertheless deserve somehow special attention because of the fact that they both are relatively rarely used and because they allowed us to get very interesting results.

The first experiment we would like to briefly describe here is the homodyne transmission system that is sketched in Fig. 3. This is the system that allowed us to obtain the results of refs. [12] and [14]. The idea is in principle quite simple: it consists in recombining on the CCD detector the emission of the sample with a delayed pulse from the exciting laser. A similar system has been recently used in order to study and manipulate the dynamics of Rabi oscillations in microcavities [46].

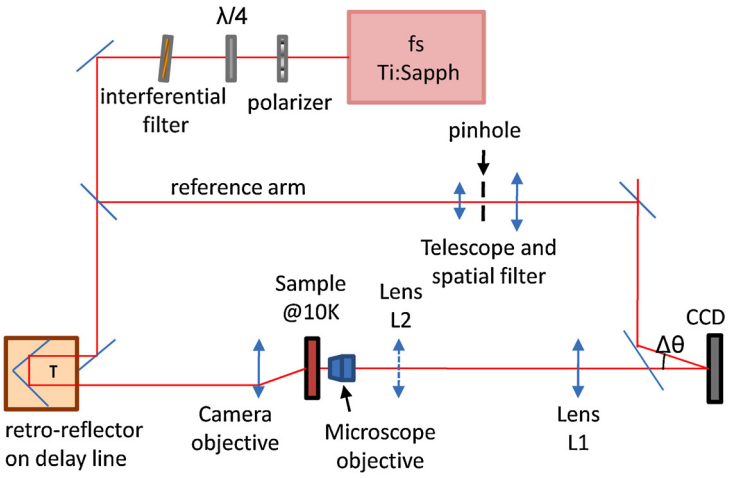


**Fig. 3.** Schematics of the homodyne system. Pulses from a Ti:sapphire laser are split into two arms. One excites the sample at a given angle, given a well-defined speed to the polariton fluid. The light emitted by the sample is interfered with the second pulse from the laser. The interference fringes are then Fourier transformed so as to obtain the time-resolved density and phase of the fluid (from the PhD thesis of Gaël Nardin [43]).

The second system has been inspired by the system installed by Wolfgang Langbein in Cardiff [47]. This is a pump&probe as well as a four-wave mixing system with heterodyne detection. The system is detailed schematically in Fig. 4. This system allows an unprecedented rejection of all sources of spurious signal and noise. It allows very high-quality results (see, for example, [48]).

## 3. Bistability

As briefly stated in the *Introduction* section, polaritons evidence interesting bistable properties allowed by the interactions of their excitonic constituents. The first observation of bistability in the case of polaritons has been obtained by the group of Élisabeth Giacobino [18]. In this initial experiment, the bistable loop was observed when moving the laser spot at the surface of the sample under resonant excitation at a very low excitation wavevector. Major improvements could be obtained by the use of confined polaritons, which allows separating the ground state of the polaritons from the excited ones. For example, the bistable behavior of a microcavity has been observed in an electrically pumped micropillar $p$–$n$ junction [19]. In this case, the bistability was in fact due to the strong-to-weak-coupling transition in the system. This bistable behavior was shown to produce propagating fronts of instability that could be used in future devices [20]. In an optical excitation experiment, the threshold of the bistability is in fact given by the equalization of the excitation laser blueshift and the density-dependent blueshift of the polariton population. When the system switches to the upper state of the bistable loop, the polaritons are basically fully resonantly excited.

Using our carefully designed mesas, it has been possible to observe bistability in an optimal fashion [29]. The adjustable separation of the different confined states, as a function of the size of the mesa, indeed allows us to precisely detune the excitation laser so as to provide at will the required bistable loop. It also allows separating the ground state from the excited ones and to tune the excitation laser to the biexciton resonance. The principle of the experiment is depicted in Fig. 5: the excitation laser (red dot on the right figure) is slightly detuned from the ground state (here in a 3-μm-diameter mesa) [50].

Typical bistable loops that have been observed for the case of a 3-μm mesa are shown in Fig. 6. The different loops have been obtained for the same laser detuning, but for different values of the ellipticity of the exciting laser [51].

In Fig. 6, the excitation power has been scanned from 0.2 to 3 mW, forward (fw) and backward (bw), with four different excitation polarization degrees indicated in the figure: $\rho_p = 0.77,\ 0.64,\ 0.17$, and 0. For large degrees of circular polarization ($\rho_p = 0.77$), the system shows a conventional bistability loop for only one spin polarization, the population in the counter circular polarization stays very small. When we decrease the polarization ($\rho_p = 0.64$), a larger population in the minority polarization now exists and the system shows some evidence of nonlinear losses. $\sigma^+$ polaritons jump to their upper branch for a power of 1.5 mW. The subsequent jump of $\sigma^-$ polaritons to their upper branch causes a very strong decrease in the population of $\sigma^+$ polaritons. This gives rise to the appearance of a middle-intensity branch. Similarly, when $\sigma^-$ polaritons jump to their lower branch, $\sigma^+$ polaritons jump back to their upper branch.

This shows that important nonlinear losses occur in the presence of polaritons of opposite spins. This loss mechanism is evidenced even better while increasing the ellipticity further ($\rho_p = 0.17$) with a larger ratio between the upper $\sigma^+$ polariton branch and the middle branch. The case of linear polarization in d) gives evidence of repulsive interactions. Indeed, the simultaneous jumps of $\sigma^+$ and $\sigma^-$ populations are the result of repulsive interactions: the blueshift of the one-spin polarization favors the blueshift of the other spin polarization.

Because of these observations, we were able to formulate the hypothesis of biexciton formation through pairing of spin-up and spin-down polaritons under elliptically or linearly polarized excitation. Biexciton states have a long radiative

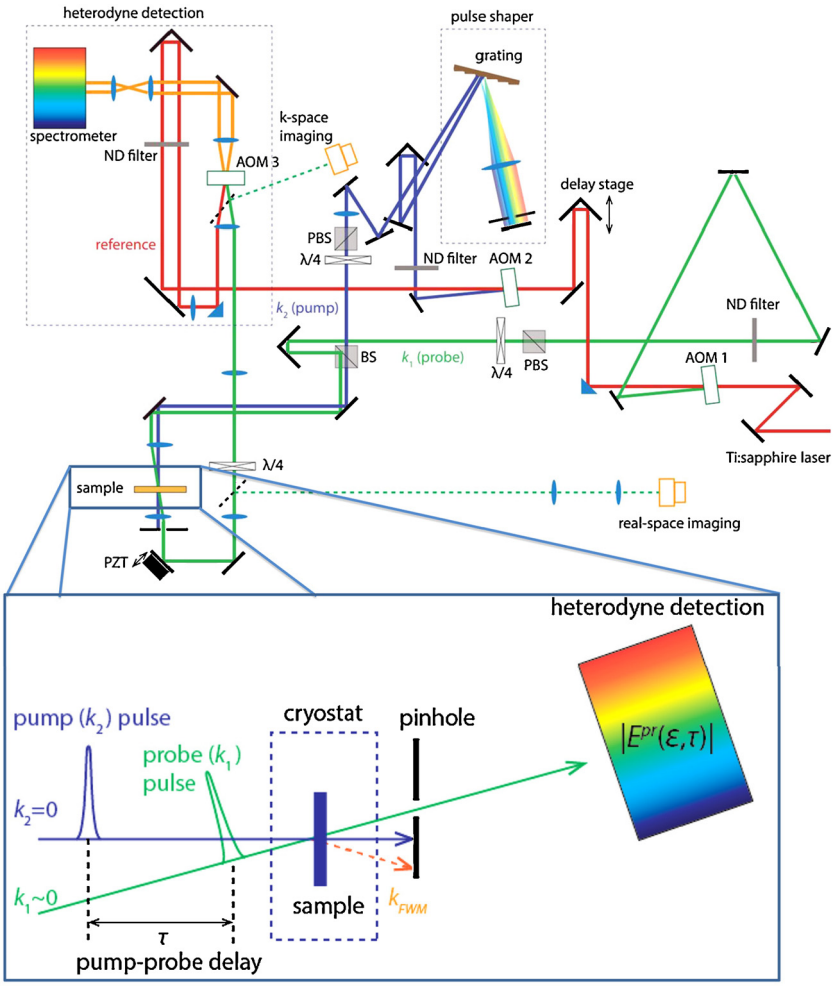


**Fig. 4.** Schematics of the heterodyne four-wave mixing system. Pulses from a Ti:sapphire laser are split into three arms. All pulses are frequency shifted to allow for synchronous detection of the proper combination. Two of the pulses are used to excite the sample and the last one is a reference that is mixed with the signal to be detected. The excitation pulse can also be shaped to the proper energy width through a pulse (from the PhD thesis of Naotomo Takemura [49]).

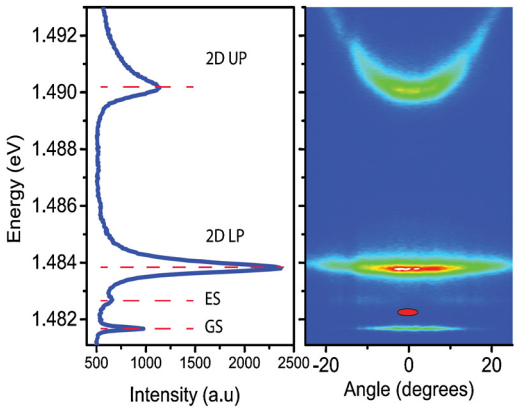


**Fig. 5.** Principle of the excitation for optimal observation of bistability with a mesa. Left: emission spectrum, right: far-field emission and laser position (from [48]).

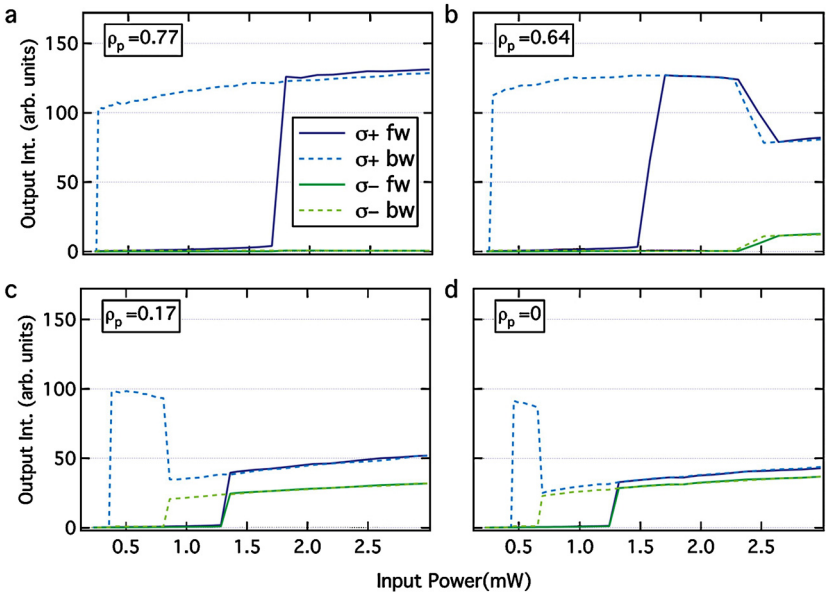


**Fig. 6.** Different bistable loops observed in a 3-μm mesa under an excitation with a laser detuning of 0.49 meV with different ellipticity values of the laser, indicated in each of the panels (from [51]); $\rho = \pm 1$ corresponds to circular polarization, $\rho = 0$ to linear polarization.

lifetime and contribute to the blueshift of both polarizations, which lowers the thresholds of bistability. This assumption will be of major importance for the observation of the Feshbach resonance.

As a standard in the field, we model the system using a Gross–Pitaevskii equation of the following form (see ref. [49] for details):

$$\mathrm{i}\frac{\mathrm{d}}{\mathrm{d}t}\psi_{\pm} = \left[\epsilon_{\mathrm{g}} - \frac{\mathrm{i}}{2}\left(\gamma + \beta|\psi_{\mp}|^2\right) + \alpha_1|\psi_{\pm}|^2 + \alpha_2|\psi_{\mp}|^2\right]\psi_{\pm} + \frac{\epsilon_{\mathrm{lin}}\psi_{\mp}}{2} + F_{\pm}\mathrm{e}^{-\mathrm{i}\omega_{\mathrm{L}}t} \tag{1}$$

In this equation, all parameters have their usual meaning: $\psi_{\pm}$ is the wavefunction of the condensate, $\epsilon_{\mathrm{g}}$ its energy, $F_{\pm}$ the amplitude of the driving field. The important parameters are the interaction constants for co- and counter-circularly polarized polaritons $\alpha_1$ and $\alpha_2$. $\gamma$ is the polariton homogeneous broadening and $\beta$ is a new coefficient that corresponds to the loss of polaritons through binding into biexcitons. As detailed in [49], a proper choice of the different parameters in this equation allows us to reproduce the main features of the experiments. The loss coefficient $\beta$ is mandatory to reproduce the switching to and from the middle branch of the bistable loop. The fitting coefficients, scaled to the value of $\alpha_1$ are the following: $\alpha_2 = 0.4\alpha_1$ and $\gamma = 0.4\alpha_1$, which differ significantly from the results published in the literature. For example, in [52] the $\alpha_2$ parameter is found to be negative and much smaller than $\alpha_1$. A more detailed study of the value of the interaction parameters in the Gross–Pitaevskii equations is therefore necessary, but before describing our efforts in that direction, let us detail the observations of the multistable behavior of confined polaritons.

## 4. Multistability

The idea that, thanks to their spinor nature, a gas of polaritons might evidence a multistable behavior was initially proposed by Nikolai Gippius [28]. The possibility of such a multistable behavior depends on a subtle balance between the different parameters of the experiment. This may be evidenced in the different panels of Figs. 6 and 7.

In Fig. 7, multistable loops are observed for different input powers as a function of the ellipticity of the incoming laser beam. Let us take Fig. 7b as an example: clearly, the system shows three stable branches, one for $\sigma^-$, one for $\sigma^+$, and one for linearly polarized polaritons. This is exactly what corresponds to multistability.

Fig. 8 provides a better understanding of the process by which multistability can be obtained. This is a pseudo-3D plot of the polarization of the system as a function of both the input power and the input ellipticity. The different bistability curves have been plotted in a quasi-3D plot in order to visualize the relation between the different ways of accessing the multistability process (see Figs. 6 and 7).

## 5. Polariton interactions and Feshbach resonance

In this section, we describe our results on the measure of the polariton interactions through pump-probe spectroscopy (these results have been detailed in ref. [53]). The main idea in this direction is to measure the energy renormalization induced by the polariton interactions through the energy shift of the probe spectrum (see Fig. 9). A circularly polarized

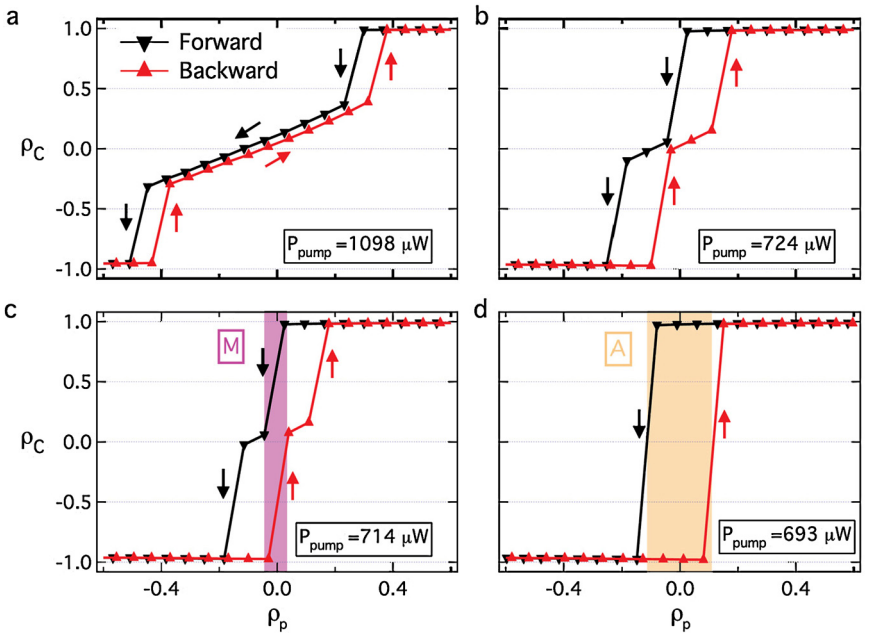


**Fig. 7.** Emission polarization degree $\rho_C$ versus the excitation polarization degree $\rho_p$. At constant excitation power, $\rho_p$ is scanned from $+0.5$ to $-0.5$ and backwards. **a.** Polarization hysteresis. At high excitation power, narrow polarization hysteresis is observed for spin-up and spin-down polaritons. On the forward path (black), a first jump of spin-up polaritons out of their upper branch causes a decrease in $\rho_C$ to a value close to $\rho_p$. Then a jump of spin-down polaritons to their upper branch brings $\rho_C$ to $-1$. On the backward path, the process is reversed with a hysteresis behavior. **b.** Effect of the excitation power. A decrease in the excitation power brings the polarization hysteresis cycles close to $\rho_p = 0$. **c.** Multistability. Further decrease of the power make the two polarization hysteresis loops merge. Three values of $\rho_C$ are allowed in the multistability region M. **d.** Spin amplification. At even lower excitation power, the overlap is complete. At the edge of the A region, a small variation of $\rho_p$ leads to a total spin-up/spin-down conversion. $\rho_C$ jumps from $+0.97$ to $-0.97$. (From the PhD thesis of Taofiq Paraiso [51].)

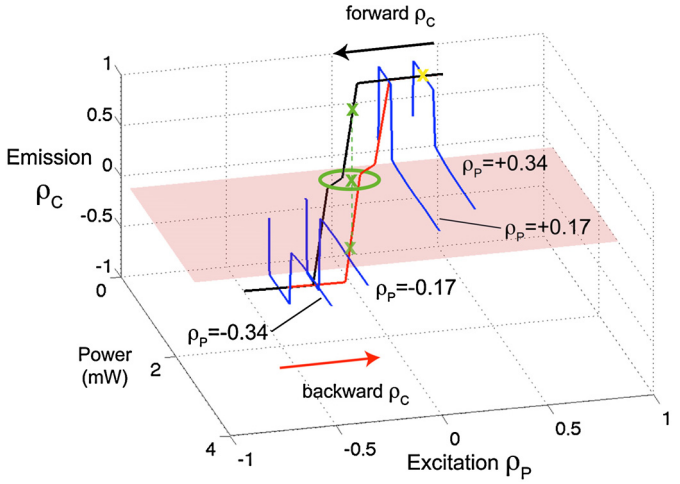


**Fig. 8.** Principle of multistability. The blue curves represent the spin conversion plateaus obtained in power-dependence experiments at different excitation polarization degrees $\rho_p = 0.34,\ 0.17,\ -0.17$, and $-0.34$. The sign of the plateau ($\pm 1$) depends on the sign of the excitation polarization degree. We represent a case where the polarization conversion is symmetric with respect to the linearly polarized excitation axis and display mirrored curves for nearly linear excitation polarization. For instance, on the $\rho_p = \pm 0.17$ curve, the polarization is converted to $\rho_C \pm 1$. Consider the system initially prepared in the yellow-cross state (fixed power) in the plateau of the $\rho_p = +0.34$ curve. The black curve highlights what happens upon a continuous change of $\rho_p$ from $+0.34$ to $-0.34$. In fact, $\rho_C$ follows the plateaus, and, eventually, polarization hysteresis in the vicinity of $\rho_p = 0$ causes the right circular polarization $\rho_C = 1$ to be preserved beyond the linearly polarized excitation axis before switching to linear $\rho_C = 0$ and then to left circular $\rho_C = -1$. Red curve: on the backward scan of $\rho_p$ (red curve), the opposite polarization $\rho_C = -1$ is preserved by hysteresis, producing a multistability region (green circle) around $\rho_p = 0$, where three spin polarization states are admitted (green crosses). (Figure adapted from the PhD thesis of Taofiq Paraiso [51].)

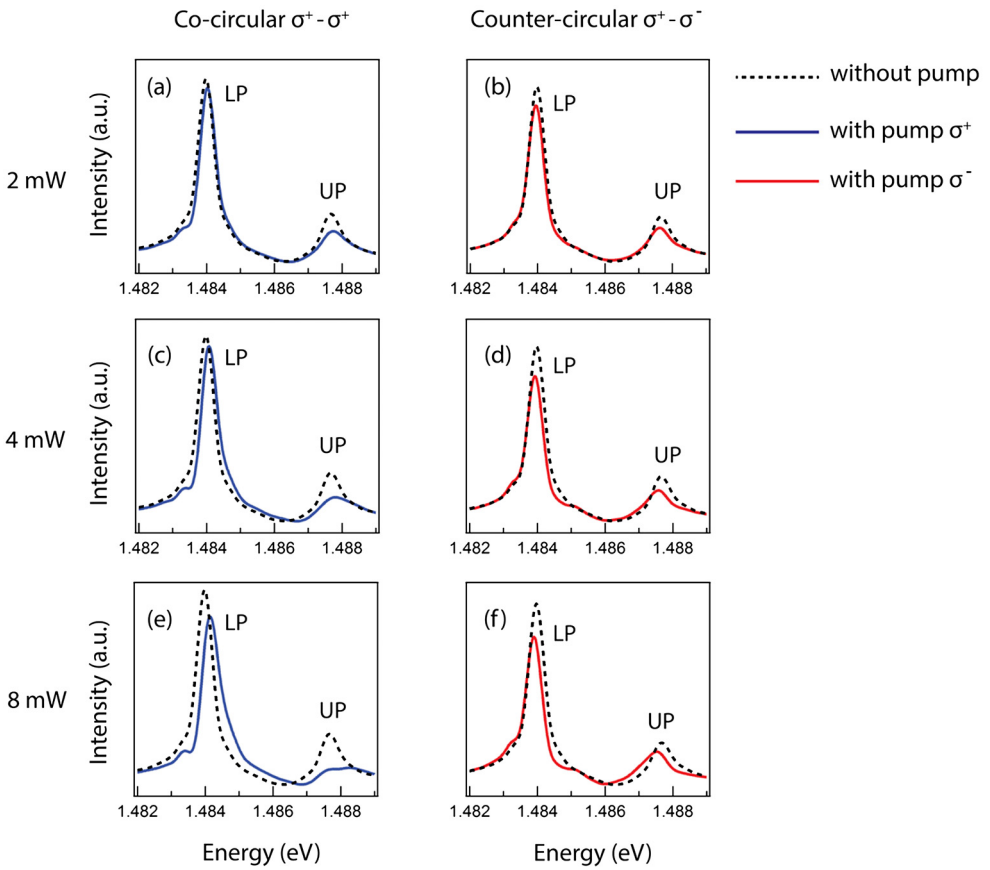


**Fig. 9.** Co (blue) and counter (red) circularly polarized pump-probe spectra at the cavity detuning of $\delta = -1.5$ meV. The spectra are plotted for three different pump intensities, as indicated in the figure. 1 mW would correspond to $1.5 \cdot 10^{13}$ photons per pulse and per cm$^2$. The probe spectra without pump and with pump pulse are respectively presented with dashed and solid lines. LP and UP respectively mean upper and lower polariton. From the PhD thesis of Naotomo Takemura [49].

strong pump pulse generates spin polarized polaritons, they are then probed with a probe pulse. Both the pump and the probe pulse have a duration of the order of 100 fs, so that their spectrum covers a range much larger than the typical splitting observed in our sample.

When the pump and probe pulse are co-circularly polarized, the energy shift of the probe pulse reflects the interaction of polaritons with parallel spins, while the energy shift of the probe for a counter-circular polarization configuration is associated with the polariton interactions with anti-parallel spins. In order to measure the coherent part of the polariton interactions, the measurements reported in Figs. 9 to 13 are performed at strictly zero time delay between the pump and the probe. Fig. 14 shows the effects of a time delay between the pump and the probe. Since the probe pulse is weak, we neglect the energy shift induced by the probe itself.

We display in Fig. 9 typical spectra for co- and counter-circular polarization for three different pump intensities, at a cavity detuning of $\delta = -1.5$ meV. Both the lower (LP) and the upper (UP) polariton blueshift in co-circular configuration. This is the clear signature of repulsive interactions between polaritons with parallel spins (see Fig. 9). As the pump intensity increases, the blueshift also increases because the energy renormalization is proportional to the population of the pump polaritons (see Eq. (1)).

In the case of negative cavity detuning, the lower polariton is photon-like, while the upper polariton is exciton-like. Since the polariton interaction originates from the excitonic part of the polariton, the blueshift is larger for the upper polariton than for the lower one.

In counter-circular polarization, both lower and upper polariton experience redshifts, which also increase with pump intensity. This signals the attractive interaction of polaritons with anti-parallel spins. Please note that the curves reported in Fig. 10 measure the effects up to the biexciton resonance, which will be described more specifically in the next paragraph.

In Fig. 10, we report the measured energy shifts of the lower and upper polaritons in co-circular configuration. The lower and upper polaritons blueshift, forming a mirror image as a function of cavity detuning: the blueshift of the lower polariton increases with cavity detuning, while the upper polariton's blueshift behaves in the opposite way. This behavior results from the respective excitonic fraction of the lower and upper polaritons. We can however notice that the mirror symmetry axis is not at zero detuning, but slightly at a negative detuning ($\approx -0.7$ meV).

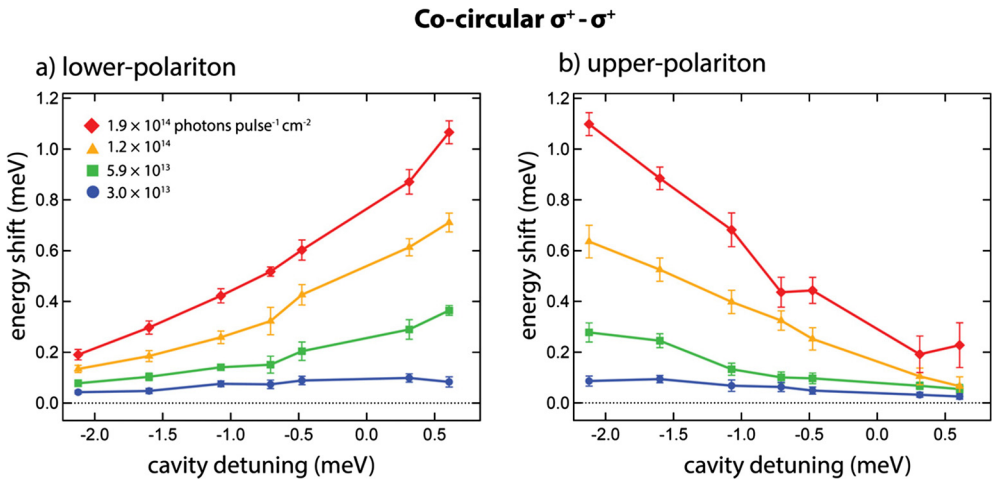


**Fig. 10.** Energy shifts of lower (a) and upper (b) polariton resonances in co-circular configuration as a function of cavity detuning. The four different symbols represent different pump intensities. From the PhD thesis of Naotomo Takemura [49].

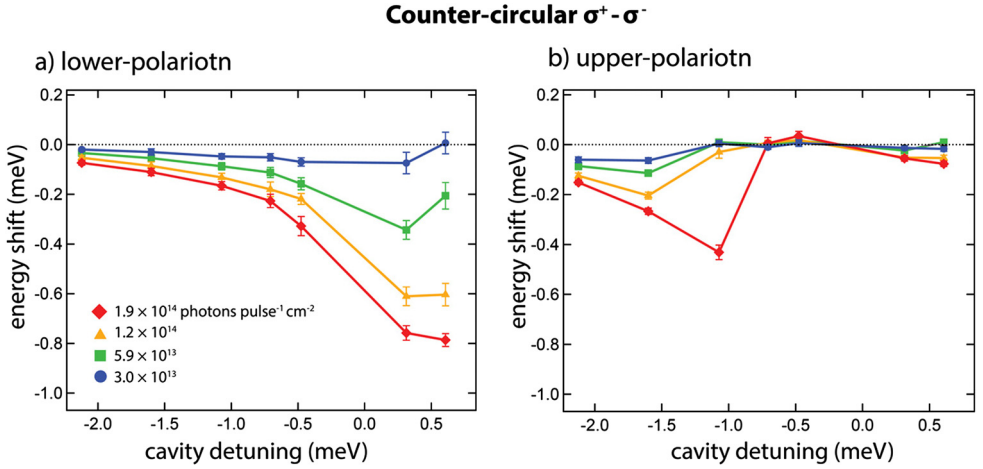


**Fig. 11.** Energy shifts of (a) lower and (b) upper polaritons in counter-circular excitation, as a function of cavity detuning. Four different symbols represent the different pump intensities. From the PhD thesis of Naotomo Takemura [49].

This shift in the symmetry axis position may have two origins: photon-assisted exchange interaction (PAE) and relaxation from the upper polariton into an exciton reservoir. PAE has been introduced by Monique Combescot in [54], and provides a detailed interpretation of the origin of exciton saturation at large densities. The former is related to the fact that PAE contributes to the attractive spinor polariton interaction between upper polaritons. The latter is associated with the possible relaxation of upper polaritons to the incoherent exciton reservoir. In order to deal with both effects properly, the excitonic Bloch equation approach would be required [55].

We report in Fig. 11 the results for the case of counter-circular configuration. Contrary to the co-circular configuration, the lower polariton energy redshifts as a result of the attractive interaction of the lower polaritons with anti-parallel spins. This behavior is a precursor of the Feshbach resonance, which will be detailed in the next section. The upper polariton presents a more complex behavior: at low pump intensity, the redshift is small for all cavity detunings, while at high pump intensities, rather large redshifts are observed for negative cavity detuning. The origin of this behavior is not yet clear.

It is worth mentioning that, at higher pump intensities, the system may reach the transition from a strong- to a weak-coupling regime. In this regime, the coherent limit description based on the Gross–Pitaevskii is not adequate to explain the experimental results. Instead, the excitonic Bloch equations (EBEs) approach including incoherent excitons (or reservoir effect) would be indispensable [56].

The theoretical description of the above results has been given in [57], and we will reproduce here the main arguments and ingredients of the model for sake of completeness. Since our experimental approach consists in exciting both lower and upper polariton states at the same time, and because we are dealing with non-linear interactions which rely on the exciton part of the polariton, cross interactions between polariton modes will be leading to a cumbersome description within the polariton basis. We have therefore decided to use the exciton–photon basis for writing the Gross–Pitaevskii

equation. Comparing the simulations to the experimental data will allow us to extract the spinor interaction constants in the exciton–photon basis Hamiltonian. In a second phase, we will discuss how to transpose our analysis in the lower polariton basis, yielding a meaningful comparison to previously reported results. The exciton–photon basis Hamiltonian is the following for the case of spin-up polaritons:

$$\hat{H} = \epsilon_c \hat{c}_\uparrow^\dagger \hat{c}_\uparrow + \epsilon_x \hat{x}_\uparrow^\dagger \hat{x}_\uparrow + \epsilon_b \hat{B}^\dagger \hat{B} + \Omega\left(\hat{c}_\uparrow^\dagger \hat{x}_\uparrow + \hat{x}_\uparrow^\dagger \hat{c}_\uparrow\right) + \hat{H}_{\text{int}} \tag{2}$$

Here $\hat{c}$, $\hat{x}$, and $\hat{B}$ are, respectively, the photon, exciton and biexciton annihilation operators, while $\hat{c}^\dagger$, $x^\dagger$ and $\hat{B}^\dagger$ are their creation counterparts. The arrows $\uparrow$ and $\downarrow$ define the spin polarization as up and down. $\epsilon_c$, $\epsilon_x$ and $\epsilon_b$ are the energies of the photon, exciton and biexciton resonances. The interacting part $\hat{\boldsymbol{H}}_{\text{int}}$ is given by:

$$\begin{aligned}\hat{H}_{\text{int}} &= \hat{H}_{\uparrow\uparrow} + \hat{H}_{\uparrow\downarrow} + \hat{H}_{\text{bx}} \\ &= g_{++}\hat{x}_\uparrow^\dagger \hat{x}_\uparrow^\dagger \hat{x}_\uparrow \hat{x}_\uparrow + g_{+-}\hat{x}_\uparrow^\dagger \hat{x}_\downarrow^\dagger \hat{x}_\downarrow \hat{x}_\uparrow + g_{\text{bx}}\left(\hat{B}\hat{x}_\uparrow^\dagger \hat{x}_\downarrow^\dagger + \hat{x}_\uparrow \hat{x}_\downarrow \hat{B}^\dagger\right)\end{aligned} \tag{3}$$

$g_{++}$ and $g_{+-}$ are the interaction strengths for parallel and antiparallel excitons. The same expressions hold when changing up and down spins in Eqs. (2) and (3). The binding of two counter polarized excitons into a biexciton is given by $g_{\text{bx}}$. This is what could be called the "*bipolariton model*" [58,59]. Please note that although related, the coefficients $g_{++}$ and $g_{+-}$ are for excitons and differ from the $\alpha_1$ and $\alpha_2$ coefficients often used to describe the non-linearities of polaritons (see, for example, Ref. [52]). Their relation will be written explicitly later in this contribution.

We could alternatively consider another type of biexciton creation mechanism: the "*giant-oscillator strength model*" [60,61]. In such a model, the biexciton possesses significant oscillator strength and is formed through the absorption of a photon in the presence of an exciton of opposite spin. Although both models could indeed be used, we favor here the bipolariton model to describe our results, because, in our study performed on polariton Feshbach resonance, we found this model to be in better agreement with our experimental findings [27].

The microscopic origin of the phenomenological interaction constants $g_{++}$ and $g_{+-}$ lies in the composite nature of excitons, which are bosons composed of electron–hole pairs. Exciton–exciton interactions are governed by the Coulomb interaction between their electron and hole constituents. The simplest approach allowing us to calculate exciton–exciton interaction with parallel spins $g_{++}$ is to compute the scattering matrix of excitons based on the Born approximation [62]. According to this calculation, for zero momentum scattering, which is the case for our experiments, the main contribution to the exciton–exciton interaction is the electron (hole) exchange interaction. However, this calculation cannot explain the existence of the exciton interaction with antiparallel spins, because the exchange interaction disappears for the excitons with antiparallel spins [43].

Therefore, the inclusion of the biexciton state through the term $g_{\text{bx}}$ and a calculation beyond the Born approximation are necessary to explain the interactions between excitons with antiparallel spins [63,64]. For example, such a calculation has been performed in Refs. [65] and [66] through the summation of higher-order interactions including the biexciton state. The result first shows that the biexciton bound state introduces resonance scattering for exciton interactions with antiparallel spins. The inclusion of these higher-order scattering matrices also results in a strong modification of the exciton–exciton interaction both for parallel and antiparallel excitons: the so-called "*continuum correlations*" [59,62]. These continuum correlations might be included in our phenomenological interaction constant with antiparallel spins $g_{\pm}$, but this goes beyond the scope of the present work, which is mainly experimental.

In our model, the phase space filling effects are omitted. Based on the results of Ref. [67], the exchange interaction of excitons with parallel spins $g_{\text{th}++}$ and the contribution from phase space filling $g_{\text{thPSF}}$ can be estimated as $g_{\text{th}++} = 3a_B e^2/\epsilon_m S$ (in the Born approximation) and $g_{\text{thPSF}} = \Omega/n_{\text{sat}} S$. Here $e$ and $\epsilon_m$ represent the elementary charge and the dielectric constant of the quantum wells. $S$ is a quantization area. Considering the 2D Bohr radius of GaAs $a_B = 6$ nm, the dielectric constant $\epsilon_m = 13.9\epsilon_0$ ($\epsilon_0$ being the vacuum permittivity), a Rabi splitting of 3.26 meV and exciton saturation density $n_{\text{sat}} = 7.5 \cdot 10^{11}$ cm$^{-2}$, we obtain a ratio $g_{\text{thPSF}}/g_{\text{th}++} = 0.23$. This ratio indicates that the Coulomb term is the dominant contribution to the repulsive interaction of polaritons with parallel spins in our sample.

Using the Heisenberg equations of motion within a mean field approximation, we obtain the equations of motion for the exciton, photon, and biexciton. In this Hamiltonian, biexcitons are created from spin-up and spin-down excitons, which indicates that counter-circular polarization configuration is mandatory to induce the biexciton effect. The exciton ($\psi_X$), photon ($\psi_C$), and biexciton ($\psi_B$) wavefunctions are described by the following exciton–photon Gross–Pitaevskii equation system:

$$i\hbar\dot{\psi}_{x,\uparrow} = \left(\epsilon_x - i\frac{\gamma_x}{2}\right)\psi_{x,\uparrow} + \Omega\psi_{c,\uparrow} + 2g_{++}|\psi_{x,\uparrow}|^2\psi_{x,\uparrow} + g_{+-}|\psi_{x,\downarrow}|^2\psi_{x,\uparrow} + g_{\text{bx}}\psi_B\psi^*_{x,\downarrow} \tag{4a}$$

$$i\hbar\dot{\psi}_{c,\uparrow} = \left(\epsilon_c - i\frac{\gamma_c}{2}\right)\psi_{c,\uparrow} + \Omega\psi_{x,\uparrow} - F \tag{4b}$$

$$i\hbar\dot{\psi}_B = \left(\epsilon_B - i\frac{\gamma_B}{2}\right)\psi_B + g_{\text{bx}}\psi_{x,\uparrow}\psi_{x,\downarrow} \tag{4c}$$

Here, $\hbar$ is the reduced Planck constant. $\gamma_X$, $\gamma_C$, and $\gamma_B$ are, the exciton, photon, and biexciton decay rates. In the numerical calculation, we use $\gamma_X = \gamma_C = 0.53$ meV. $F$ represents the external source of photons given by the laser pulse. Of course, all equations are k-dependent, which is implicitly included here.

In the co-circular polarization configuration, only the $g_{++}$ term is involved. We omit the spin index since all polariton spins are the same. Our co-circular polarization pump-probe configuration is equivalent to that of $\chi^3$ type parametric amplification. Thus, if we assume that the pump and probe beams have momentum $k_{pu} = 0$ and $k_{pr}$, respectively, an idler beam appears with a momentum $k_i = 2k_{pu} - k_{pr} = -k_{pr}$. Since in the experiment $k_{pr} = 0$, we neglect the dispersion of photons. We substitute the wave function:

$$\psi_{x(c)} = \psi^{pu}_{x(c)} + \psi^{pr}_{x(c)} e^{ikx} + \psi^{i}_{x(c)} e^{-ikx} \tag{5}$$

into the exciton–photon Gross–Pitaevskii equations (4a) and (4b). Assuming a strong pump:

$$\left|\psi^{pu}_{x(c)}\right| \gg \left|\psi^{pr,i}_{x(c)}\right|$$

the feedback on the pump wave function from the signal and idler can be discarded. Thus the pump wave function $\psi^{pu}_{x(c)}$ can be written as Eqs. (4a) and (4b). Additionally, we neglect the terms that do not conserve momentum. The dynamics of the set of wave functions $\vec{u} = (\psi^{pr}_x, \psi^{pr}_c, \psi^{i*}_x, \psi^{i*}_c)$ can be described as $i\hbar\dot{u} = M^{++}\vec{u} - \vec{F}^{pr}$ [68], where $\vec{F}^{pr}$ represents the probe pulse excitation. The matrix $M^{++}$ is given by:

$$M^{++} = \begin{pmatrix} \epsilon_x + 4g_{++}|\psi^{pu}_x|^2 - i\gamma_x/2 & \Omega & 2g_{++}\psi^{pu2}_x & 0 \\ \Omega & \epsilon_c - i\gamma_c/2 & 0 & 0 \\ -2g_{++}\psi^{pu*2}_x & 0 & -(\epsilon_x + 4g_{++}|\psi^{pu}_x|^2) - i\gamma_x/2 & -\Omega \\ 0 & 0 & -\Omega & -\epsilon_c - i\gamma_c/2 \end{pmatrix} \tag{6}$$

Since the lower and upper polaritons are excited with spectrally broad femtosecond pulses, we model the pump and probe photon pulses as instantaneous delta function pulses exciting the system simultaneously. By Fourier transforming the temporal photon probe wavefunctions, we obtain the spectra of the light emitted out of the cavity. Subtracting the pump-probe spectra from the reference spectra, we single out the energy shift of both lower and upper polariton resonances due to the presence of the pump pulse. The strength of our method to extract spinor interaction constants is based on the joint comparison of lower and upper polariton energy shifts.

As detailed in Ref. [53], the comparison between the experimental results and the computed ones are very good for a value of $g_{++} = 1$ meV$/n_0$. Here, $n_0$ is a normalization particle density for the excitation pump photon density. The lower polaritons show an increase in the energy shift from negative to positive cavity detuning, while the upper polaritons energy shift decreases. In fact, the lower polariton becomes more excitonic and the upper polariton becomes more photonic for increasing cavity detuning. This highlights the role of the excitonic content in polariton interactions.

## 6. Feshbach resonance

Lets now focus on the counter-circular configuration and concentrate on the detuning for which a crossing with the biexciton resonance occurs. Indeed, this might allow us to explore a possible Feshbach resonance for polaritons [54]. A Feshbach resonance is a scattering resonance, which occurs when the energy of two free particles reaches that of a molecular bound state [69]. In the vicinity of the resonance, the interaction strength of the two interacting particles dramatically changes.

In cold atoms, the Feshbach resonance is an essential tool to control the atom–atom interactions. It is even possible to switch the sign of atomic interactions from repulsive to attractive. For example, the instability and explosion of Bose–Einstein condensates have been realized with an attractively interacting Bose gas [70]. Moreover, in degenerate fermionic cold atomic gases, the BEC–BCS crossover has been observed by tuning the atomic interaction from repulsive to attractive [71].

In order to investigate the experimental signatures of the Feshbach resonance for polaritons, we need to work in the coherent regime where the effects are expected. Therefore we set a zero delay between pump and probe. As in the previous paragraph, we measure both the transmitted probe energy shift and amplitude change induced by the presence of the polariton population generated by the pump. We then change the detuning by moving the excitation laser across the wedge of the sample. The pump intensity is set to be large enough to produce a measurable shift ($5 \cdot 10^{10}$ polaritons/cm$^2$), but still below the transition to the weak coupling regime.

We report on the main results of this study [27] in Fig. 13, with the energy shift on the left and the absorption changes on the right, as a function of the position on the sample (plotted here in terms of detuning between the exciton and the photon energies). The total energy of two lower polaritons should cross the biexciton energy for a positive detuning of about 0.5 meV as indicated by the green shaded area in the figure.

The energy shift clearly shows a dispersive shape, characteristic of resonant scattering around a Feshbach resonance. In cold atomic systems, the dispersive shape diverges in the case of magnetic field induced Feshbach resonance, thanks to the very long molecular lifetime [53]. The smoothened dispersive shape that we observe here is similar to what is observed

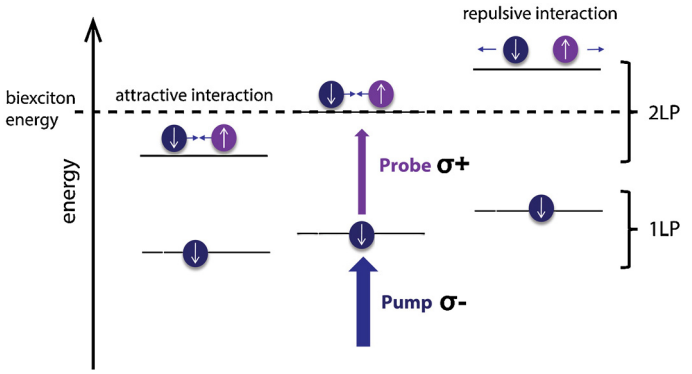


**Fig. 12.** Schematics of the pump-probe experiments around the Feshbach resonance. A population of spin-down polaritons is created by the pump pulse, then the probe introduces a few spin-up polaritons, which interact with the spin-down polaritons. The relative energy position with respect to the biexciton state determines the sign of interactions: from attractive (below the biexciton energy) to repulsive (above the biexciton energy). (From the PhD thesis of Naotomo Takemura [49].)

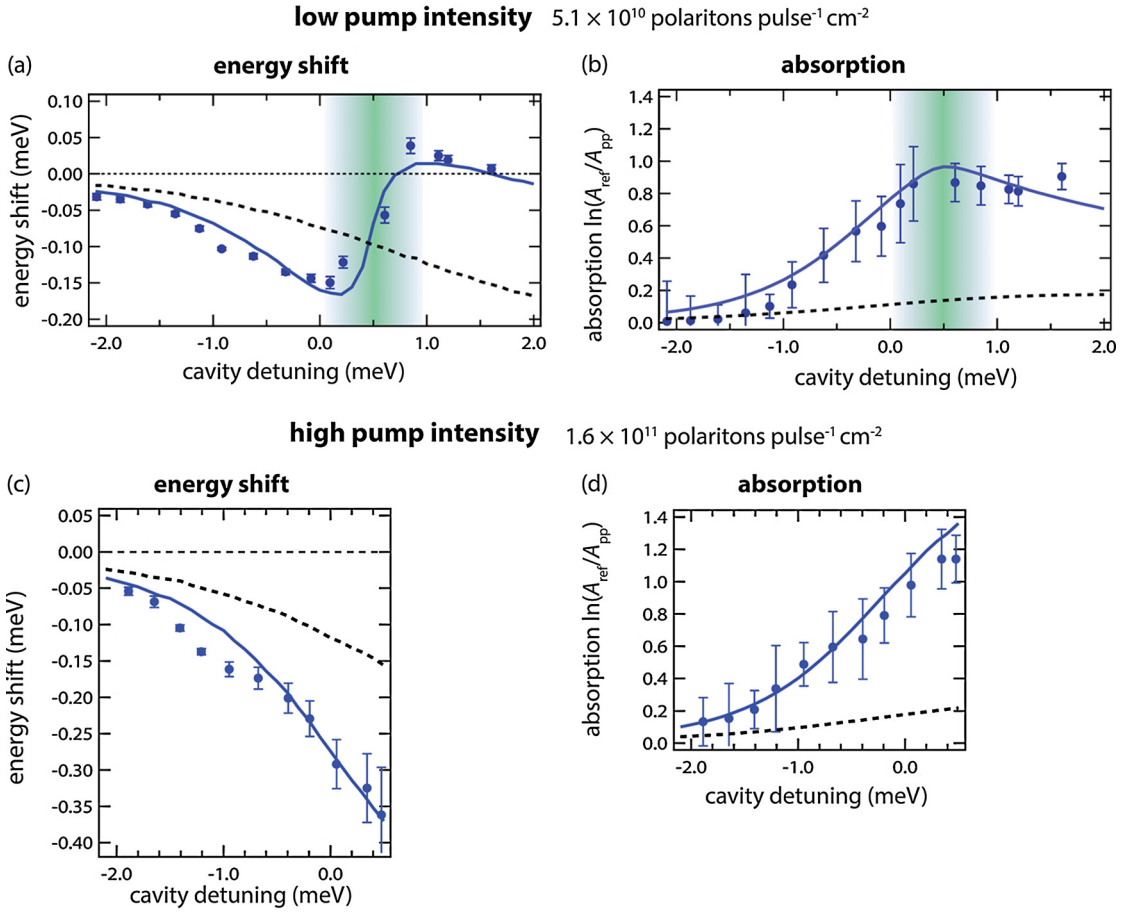


**Fig. 13.** Energy shifts (a, c) and absorption (b, d) of the pump spectrum as a function of cavity detuning. The intensities of pump polaritons are $5 \cdot 10^{10}$ (a, b) and $1.6 \cdot 10^{11}$ (c, d) polaritons/pulse/cm$^2$. The blue dots are the experimental results, the solid and dashed lines are numerical simulations respectively with and without the biexciton effect. The green shaded areas represent the expected position of the biexciton resonance. For the numerical calculation, we use the parameters given in the text. (From the PhD thesis of Naotomo Takemura [49].)

for optical Feshbach resonances with finite molecular lifetime [72]. This shape is linked with the finite lifetime of the intermediate states.

For polaritons, the finite lifetime of the molecular biexciton state prevents the dispersive shape form diverging at resonance. Nevertheless, the sign of the energy shift does change from attractive at negative detuning to positive around the biexciton resonance. At the same time, the absorption strength changes quite dramatically, which provides evidence for

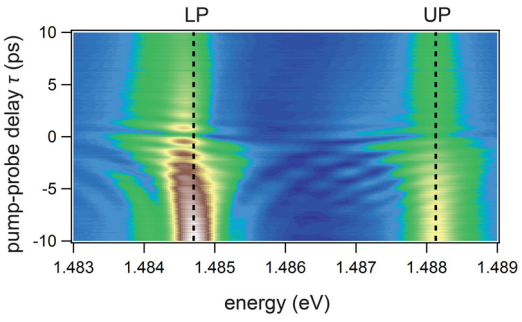


**Fig. 14.** Experimental probe transmission spectrum as a function of energy and time delay between pump and probe pulse. The cavity detuning is set at 0.5 meV. The black dashed lines are the lower and upper-polariton peak energies without pump pulse. (From the PhD thesis of Naotomo Takemura [49].)

the loss mechanism hypothesized in our observations of spinor bistability (see above). Both measured shapes provide clear evidence for a Feshbach resonance.

We now display in Fig. 14 the amplitude of the $\sigma^-$ probe spectrum as a function of the pump-probe delay at the cavity detuning 0.5 meV. We see that the redshift and absorption both remain for long delays at positive pump-probe delays. On the other hand, at negative delays, both the redshift and the absorption decrease with the increase of the delay, which is the expected behavior in the coherent limit model for the Feshbach resonance. In order to simulate the probe behavior at positive delays, we would need to include the incoherent population effect of excitons [52].

To retrieve the physics behind our observations, we have performed numerical simulations based on a two-channel model, which includes coupling between polariton and biexciton $g_{\mathrm{BX}}$ in addition to the normal mode coupling between exciton and photon $\Omega_{\mathrm{X}}$. For our system, it is given by the following Hamiltonian [73,74]:

$$H = \Omega_{\mathrm{X}}\left(a_{\mathrm{c}\sigma}\,\psi^{+}_{\mathrm{X}\sigma} + a_{\mathrm{c}\sigma}\,\psi_{\mathrm{X}\sigma}\right) + \frac{U_{\mathrm{bg}}}{2}\left(\psi^{+}_{\mathrm{X}\sigma}\,\psi^{+}_{\mathrm{X}-\sigma}\,\psi_{\mathrm{X}-\sigma}\,\psi_{\mathrm{X}\sigma}\right) + g_{\mathrm{BX}}\left(\psi^{+}_{\mathrm{BX}}\psi_{\mathrm{X}\sigma}\,\psi_{\mathrm{X}-\sigma} + \psi_{\mathrm{BX}}\psi^{+}_{\mathrm{X}\sigma}\,\psi^{+}_{\mathrm{X}-\sigma}\right) \tag{7}$$

In this Hamiltonian, $a_{\mathrm{c}\sigma}$ and $\psi_{\mathrm{X}\sigma}$ ($a^{\dagger}_{\mathrm{c}\sigma}$ and $\psi^{\dagger}_{\mathrm{X}\sigma}$) are respectively the photon and exciton annihilation (creation) operators. The polarization states of the photon and of the exciton are defined by the spin variable $(\sigma, -\sigma)$ as $(\uparrow, \downarrow)$. The coefficient $g_{\mathrm{BX}}$ sets the strength of the possible coupling between two polaritons with antiparallel spins and one biexciton through the Coulomb interaction of their excitonic content. $U_{bg}$ represents the value of the phenomenological interaction between polaritons with anti-parallel spin usual referred to as the background interaction.

There are several possible mechanisms that may contribute to this "*background interaction*". First, the indirect scattering through dark exciton states has been considered [75,76], and possibly the scattering through excited exciton states [77], as well as exciton–exciton scattering continuum correlations [78], all of which are attractive. Repulsive interactions have also been considered such as Van-der-Waals and electrostatic interactions [62] could also contribute. However, it is very difficult to determine a priori their relative contributions and the global attractive nature is only phenomenological, allowing us to fit the negative detuning part of our observations.

Within a mean-field approximation, this effective quadratic Hamiltonian may be embodied with the following $3 \times 3$ matrix which includes the spin-up probe operators and the biexciton amplitude:

$$\hat{H}_{\mathrm{eff}} = [\,\hat{\psi}_{x,\uparrow} \quad \hat{\psi}_{\mathrm{c},\uparrow} \quad \hat{\psi}_{\mathrm{B}}\,]^{\dagger} \begin{bmatrix} \epsilon_x + g_{+-}n_{x,\downarrow} - \mathrm{i}\gamma_x & \Omega & g_{\mathrm{bx}}\sqrt{n_{x,\downarrow}} \\ \Omega & \epsilon_c - \mathrm{i}\gamma_c & 0 \\ g_{\mathrm{bx}}\sqrt{n_{x,\downarrow}} & 0 & \epsilon_{\mathrm{B}} - \mathrm{i}\gamma_{\mathrm{B}} \end{bmatrix} \tag{8}$$

where $n_{x,\downarrow}$ represents the density of the pump exciton, which we assume to be given by:

$$n_{x,\downarrow} = \frac{n_{\mathrm{p}}}{2}\left(1 + \frac{\delta}{\sqrt{\delta^2 + \Omega^2}}\right) \tag{9}$$

The simulated energy shift and absorption changes are displayed in Fig. 15 as solid lines for the following parameters:

$$g_{\mathrm{bx}} = 0.36\frac{\mathrm{meV}}{\sqrt{n_0}} \qquad U_{\mathrm{bg}} = -0.18\frac{\mathrm{meV}}{n_0}$$

These are the parameters that give the best fit to the experimental observations. To be complete, we also show as a dashed line in the same figure the simulation obtained with the background interaction alone. Clearly, this background interaction is attractive, but it changes monotonically with detuning and cannot reproduce the dispersive shape of the energy shift. At the same time, the background interaction does not give rise to a sizeable absorption, which clearly comes from the binding of two polaritons into a biexciton. The other way around, without the background interaction, the energy shift would become strongly positive above the biexciton resonance. Clearly, both interactions have to be taken into account.

In order to highlight the resonance due to the exciton–biexciton coupling, we plot in Fig. 16 the ratios for the energy shift as well as for the absorption for the two cases of biexciton resonance only and background interaction only. These

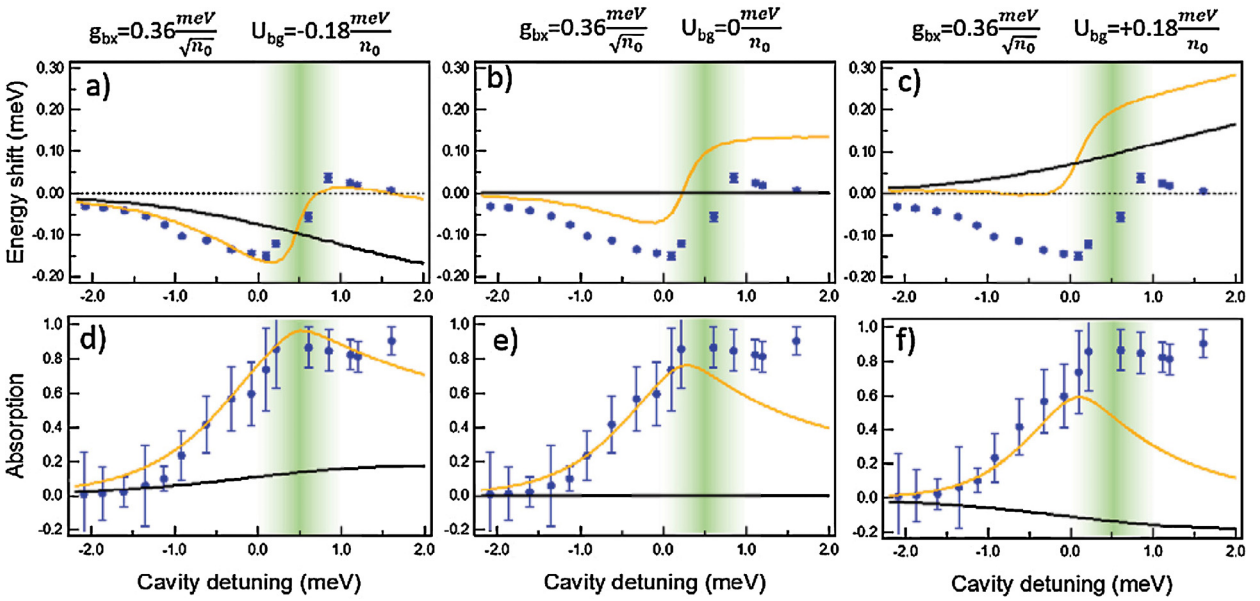


**Fig. 15.** Effect of the value of the background interaction constant on the quality of the fit reported in Fig. 13. The upper panel displays, as a function of cavity detuning, the computed energy shifts and the lower panel, the absorption strength. The experimental results are the blue dots. The orange and black lines report the numerical simulations with and without polariton–biexciton coupling, respectively. (From ref. [27], supplementary material.)

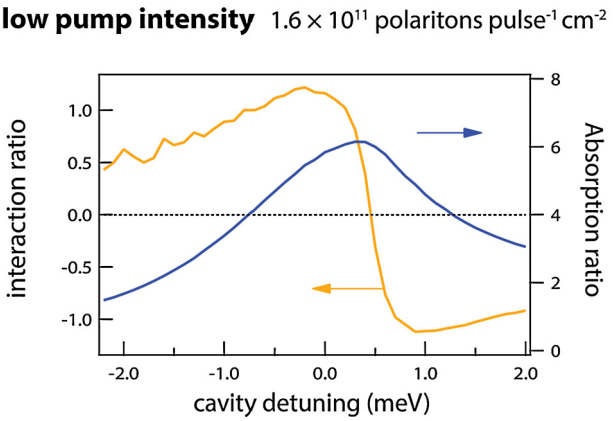


**Fig. 16.** Interaction (orange line) and absorption (blue line) ratios as a function of the cavity detuning. The interaction and absorption ratios are the ratios between the solid (with $g_{bx} \neq 0$) and dashed ($g_{bx} = 0$) lines extracted from Fig. 13. (From the PhD thesis of Naotomo Takemura [49].)

ratios are calculated from the numerical plots in Fig. 13. The interaction and absorption ratios are obtained by dividing the total contribution (solid curve) by the background contribution (dashed curves). The two ratios show the familiar behavior of a scattering resonance. The interaction ratio (orange curve) displays a dispersive shape and a large variation both in sign and in amplitude with respect to the resonance point. The profile of the absorption ratio (blue curve) also displays a typical enhancement of the absorption at the resonance associated with the two-body loss process of lower polaritons. A similar behavior has been reported for optical Feshbach resonance in $^{87}$Rb condensates [57].

Let us now concentrate on the coupling between polaritons and biexcitons in the matrix of the effective Hamiltonian (Eq. (3)). This coupling is given by a coefficient that amounts to $g_{bx}\sqrt{n_{x,\downarrow}}$ and therefore depends also on the population of polaritons in the system. In the low-density regime, this coefficient is much smaller than the decay rate of biexcitons: $g_{bx}\sqrt{n_{x,\downarrow}} << \gamma_B$, which allows the energy shift to display the smooth dispersive lineshape shown in Fig. 13a. In the high-density regime, the situation becomes different and the biexciton coupling strength becomes dominant. Fig. 17 shows the experimental spectra in the high-excitation density regime.

In Fig. 18, we plot the position of the two peaks observed in Fig. 17b as a function of the cavity detuning, for a large density of $1.6 \times 10^{11}$ polaritons/pulse/cm$^2$.

The experimental results are compared to the results of the simulation with (continuous lines) and without (dashed lines) biexciton coupling. We associate the appearance of the two resonances with "*strong coupling*" between the photon mode and the biexciton resonance [79]. Since the biexciton coupling term depends on the pump polariton population as

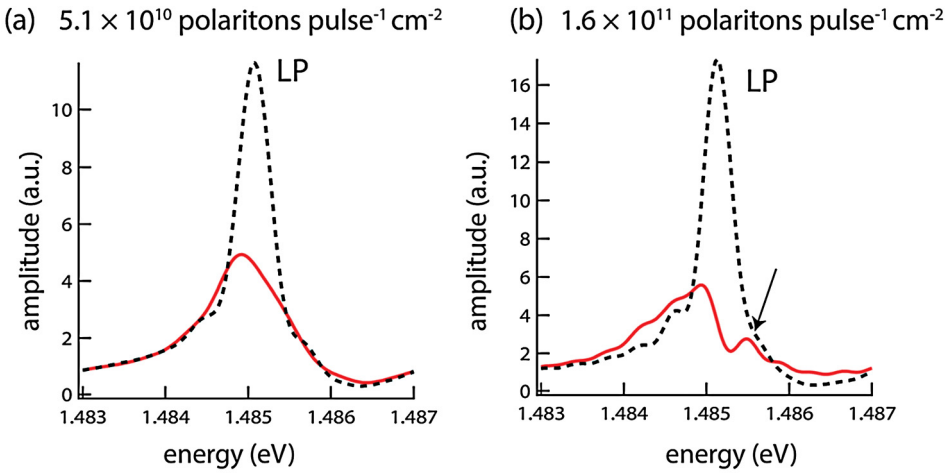


**Fig. 17.** Comparison of pump-probe spectra for different pump densities: the dashed curves correspond to a non-excited cavity. Figure (a) shows the low-pump case, where a redshift of the probe is observed, together with strong absorption. In (b), larger pump intensity is used and the spectrum shows a clear splitting that is reported as a function of detuning in Fig. 18. Here, cavity detuning is ±0.25 meV. From the PhD thesis of Naotomo Takemura [47].

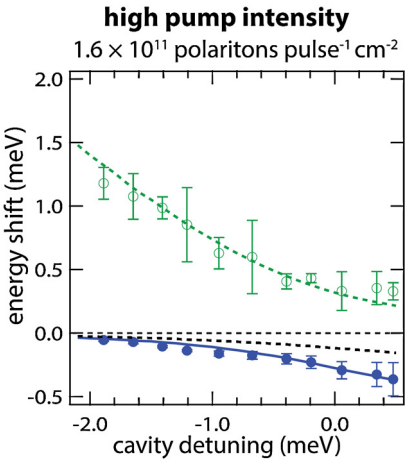


**Fig. 18.** Energy shifts of the two peaks (green open circles and blue dots) shown in Fig. 17 as a function of cavity detuning. The solid lines and dashed lines are numerical simulations respectively with and without the biexciton coupling. From the PhD thesis of Naotomo Takemura [47].

$g_{\mathrm{bx}}\sqrt{n_{\mathrm{x},\downarrow}}$, at large polariton densities, polariton–biexciton coupling becomes comparable to the linewidth of the involved states. Fig. 18 might therefore be interpreted as an "*anti-crossing*" between the lower-polariton and the biexciton resonance.

## 7. Lower polariton interaction constants

When experiments with lower polaritons are considered, a continuous wave laser excitation is usually involved. In order to compare the parameters that we have extracted to this new configuration, we need to transform the exciton–photon basis Hamiltonian into lower-polariton Hamiltonian. To this aim, we first rewrite the Hamiltonian of Eq. (2) using the lower polariton basis defined as $\hat{p}_{\mathrm{lp}} = X\hat{x} + C\hat{c}$ and neglect all terms that include upper polaritons [63]:

$$\begin{aligned}\hat{H} &= \epsilon_c \hat{c}_\uparrow^\dagger \hat{c}_\uparrow + \epsilon_x \hat{x}_\uparrow^\dagger \hat{x}_\uparrow + \Omega\left(\hat{c}_\uparrow^\dagger \hat{x}_\uparrow + \hat{x}_\uparrow^\dagger \hat{c}_\uparrow\right) + \hat{H}_{\mathrm{int}} \\ &\simeq \epsilon_{\mathrm{lp}} \hat{p}_{\mathrm{lp}}^\dagger \hat{p}_{\mathrm{lp}} + g_{++}|X|^4 \hat{p}_{\mathrm{lp},\uparrow}^\dagger \hat{p}_{\mathrm{lp},\uparrow}^\dagger \hat{p}_{\mathrm{lp},\uparrow} \hat{p}_{\mathrm{lp},\uparrow} + g_{+-}|X|^4 \hat{p}_{\mathrm{lp},\uparrow}^\dagger \hat{p}_{\mathrm{lp},\downarrow}^\dagger \hat{p}_{\mathrm{lp},\downarrow} \hat{p}_{\mathrm{lp},\uparrow} \\ &\quad + g_{\mathrm{bx}}\left(X^2 \hat{p}_{\mathrm{lp},\uparrow} \hat{p}_{\mathrm{lp},\downarrow} \hat{B}^\dagger + X^{*2} \hat{p}_{\mathrm{lp},\uparrow}^\dagger \hat{p}_{\mathrm{lp},\downarrow}^\dagger \hat{B}\right)\end{aligned} \tag{10}$$

where $X$ and $C$ are the Hopfield coefficients of the lower polariton, as usual. The lower polariton energy $\epsilon_{\mathrm{lp}}$ is then given by:

$$\epsilon_{\mathrm{lp}} = \frac{\epsilon_{\mathrm{c}} + \epsilon_{\mathrm{x}}}{2} - \frac{1}{2}\sqrt{(\epsilon_{\mathrm{c}} - \epsilon_{\mathrm{x}})^2 + \Omega^2} \tag{11}$$

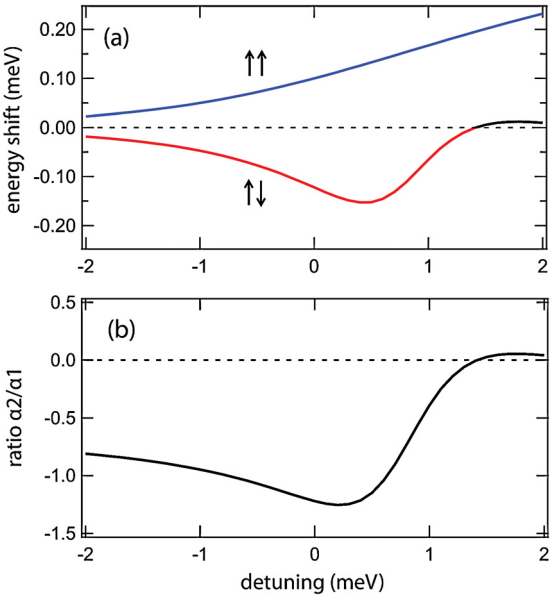


**Fig. 19.** (a) Computed polariton energy shift for co-circular (blue) and opposite spins (red) as a function of the cavity detuning for a normalized pump polariton density of 0.2; (b) $\alpha_2/\alpha_1$ ratio as a function of cavity detuning (from Ref. [53]).

As usual, we calculate the Heisenberg equations of motion applying mean-field approximation. This brings us to:

$$i\hbar\dot{\psi}_{lp,\uparrow} = \left(\epsilon_{lp} - i\frac{\gamma_{lp}}{2}\right)\psi_{lp,\uparrow} + 2g_{++}|X|^4|\psi_{lp,\uparrow}|^2\psi_{lp,\uparrow} + g_{+-}|X|^4|\psi_{lp,\downarrow}|^2\psi_{lp,\uparrow} + g_{bx}X^{*2}\psi^*_{lp,\downarrow}\psi_B - F \tag{12}$$

and

$$i\hbar\dot{\psi}_B = \left(\epsilon_B - i\frac{\gamma_B}{2}\right)\psi_B + g_{bx}X^2\psi_{lp,\uparrow}\psi_{lp,\downarrow} \tag{13}$$

where $\gamma_{lp} = |C|^2\gamma_c + |X|^2\gamma_x$ is the lower polariton decay rate. We will now solve Eqs. (12) and (13) for parallel spins and then antiparallel spins. For the parallel spin configuration, the dynamics of the lower polariton wave function $\psi_{lp}$ is given by:

$$i\hbar\dot{\psi}_{lp} = \left(\epsilon_{lp} - i\frac{\gamma_{lp}}{2}\right)\psi_{lp} + 2g_{++}|X|^4|\psi_{lp}|^2\psi_{lp} - F \tag{14}$$

Thus, the mean-field energy shift simply becomes:

$$\Delta E_{++} = \alpha_1|\psi_{lp}|^2 \tag{15}$$

Where the square of the polariton wavefunction $|\psi_{lp}|^2$ gives the lower polariton density. The lower polariton interaction with parallel spins is thus defined as:

$$\alpha_1 = 2g_{++}|X|^4 \tag{16}$$

In Fig. 19a, we plot as a blue line the energy shift of the lower polariton for parallel spin interaction (Eq. (16)) using the value of $g_{++}$ that fits best our experimental results and a normalized pump polariton density $|\psi_{lp}|^2 = 0.2$. The energy shift follows the expected dependence given by the excitonic content of the lower polariton through the term $|X|^4$.

In order to obtain the lower polariton interaction for antiparallel spins, we consider pump-probe spectroscopy in the counter-circular polarization configuration. Assuming that the spin-up pump pulse is much stronger than the spin-down probe pulse, we can express the probe lower polariton dynamics as $i\hbar\dot{u} = M\vec{u} - \vec{F}^{pr}$, where $\vec{u} = (\psi^{pr}_{lp\downarrow}, \psi_B)$ and $\vec{F}^{pr}$ is a source term. The matrix $M$ is then:

$$M = \begin{pmatrix} \epsilon_{lp} + g_{+-}|X|^4|\psi^{pu}_{lp\uparrow}|^2 - i\gamma_{lp}/2 & g_{bx}X^{*2}\psi^{pu*}_{lp\uparrow} \\ g_{bx}X^2\psi^{pu}_{lp\uparrow} & \epsilon_B - i\gamma_B/2 \end{pmatrix} \tag{17}$$

Let us consider a pump resonant at the lower polariton energy, then it may be written $\psi^{pu}_{lp\uparrow} = |\psi^{pu}_{lp\uparrow}|e^{-i\epsilon_{lp}t/\hbar}$, and the probe has energy $\epsilon : \vec{F}^{pr} = (0, 1)e^{-i\epsilon t/\hbar}$. In order to obtain the steady-state solutions, we assume that the pump wave function has

the form $\psi^{pu}_{lp\downarrow} = \psi^{pu}_{lp\downarrow}(\epsilon)e^{-i\epsilon_{lp}t/\hbar}$ and that the biexciton wavefunction can be expressed as $\psi_B = \psi_B(\epsilon)e^{-i(\epsilon+\epsilon_{lp})t/\hbar}$. Replacing $\psi^{pu}_{lp\uparrow}$ and $\psi^{pu*}_{lp\uparrow}$ by $|\psi^{pu}_{lp\uparrow}|$ in the matrix $M$, we obtain the steady-state solution of the probe lower-polariton spectrum:

$$\psi^{pr}_{lp\downarrow}(\epsilon) = (1 \quad 0)\left[M - \begin{pmatrix} \epsilon & 0 \\ 0 & \epsilon_{lp}+\epsilon \end{pmatrix}\right]^{-1}\begin{pmatrix} 1 \\ 0 \end{pmatrix}. \tag{18}$$

The analytic solution for $\psi^{pr}_{lp\downarrow}(\epsilon)$ is then:

$$\psi^{pr}_{lp\downarrow}(\epsilon) = \left[\epsilon_{lp} - \epsilon + g_{+-}|X|^4|\psi^{pu}_{lp\uparrow}|^2 - i\gamma_{lp}/2 - \frac{g^2_{bx}|X|^4|\psi^{pu}_{lp\uparrow}|^2}{\epsilon_B - \epsilon_{lp} - \epsilon - i\gamma_B/2}\right]^{-1}. \tag{19}$$

Under the assumption of a weak exciton–biexciton coupling and a low pump excitation density, the two-mode solutions of $\psi^{pu}_{lp\downarrow}(\epsilon)$ may be approximated by a single solution. Indeed, substituting $\epsilon = \epsilon_{lp}$, the pump induced energy shift $\Delta E_{+-}$ can be approximated as:

$$\Delta E_{+-} \simeq g_{+-}|X|^4|\psi^{pu}_{lp\uparrow}|^2 - \frac{g^2_{bx}|X|^4|\psi^{pu}_{lp\uparrow}|^2(\epsilon_B - 2\epsilon_{lp})}{(\epsilon_B - 2\epsilon_{lp})^2 + (\gamma_B/2)^2} \tag{20}$$

and the interaction between lower polariton with antiparallel spins is then:

$$\alpha_2 \simeq g_{+-}|X|^4 - \frac{g^2_{bx}|X|^4(\epsilon_B - 2\epsilon_{lp})}{(\epsilon_B - 2\epsilon_{lp})^2 + (\gamma_B/2)^2} \tag{21}$$

This result shows that the two contributions to the energy shift in the counter-polarized configurations bring strong similarity to derived expressions for optical Feshbach resonance in cold atoms. The first term is proportional to the excitonic content $|X|^4$, this term is due to the interaction between antiparallel spin polaritons is usually called the background interaction term (see discussion above). The second term takes the form of a Lorentzian profile. The values taken by $\alpha_2$ are reported in Fig. 19a for a normalized pump density of 0.2. The energy shift displays a change in sign and amplitude when the energy of two lower polaritons crosses the energy of the biexciton, as observed in the experiments reported above.

In Fig. 19b, we plot the ratio between counter- and co-polarized interactions. We obtain a ratio similar to the one reported previously using a different approach [51]. For negative detuning, the ratio takes a negative value, $-0.8$, which progressively increases until reaching $-1.2$, then changes suddenly to a slightly positive value. This comparison to previous results strengthens the interest and generality of the method presented here.

## 8. Conclusions

In this review, we have described a series of experiments that highlight the rich variety of phenomena that are allowed by the partial excitonic origin of polaritons. Both the interaction between polaritons and the influence of spin on these interactions have been considered. Of particular interest are the possibility of a multistable behavior of polaritons and the existence of a Feshbach resonance at the crossing between the energy of two lower polaritons and one biexciton. The experiments have been modeled within two frameworks: the exciton–photon–biexciton basis and the polariton–biexciton basis.

## Acknowledgements

This work is inspired from the successive PhD works in my group over the past 15 years, starting from the PhD thesis of Michele Saba, when we first envisaged the possibility of condensation of polaritons and designed an original way to produce efficient trapping of polaritons. This work has been followed by what I call the dream team of LOEQ with, in order of appearance onstage, Stefan Kundermann, Reda Idrissi Kaitouni, Ounsi El Daïf, Konstantinos Lagoudakis, Roland Cerna, Verena Kohnle, Francesco Manni, Gabriele Grosso. More specifically, the experiments reported here were performed and analyzed by Gael Nardin, Taofiq Paraiso, and Naotomo Takemura. This work has also been supported very efficiently by a group of extremely talented postdoctoral fellows, whom I wish to congratulate warmly for their outstanding work: Maxime Richard, Augustin Baas, Thierry Guillet, Barbara Pietka, Yoan Léger, Stéphane Trébaol, Mitchell Anderson, and Gregory Sallen. Last, but not least, the constant and careful supervision of the group by Marcia Portella-Oberli, and more recently by Daniel Oberli has been a major contribution to the success of the enterprise. I also would like to convey my most sincere thanks to the theoreticians who allowed us to understand our results, by spending enough time with us, and by putting into simple words the results of their equations. In particular, Cristiano Ciuti, Vincenzo Savona, Michiel Wouters, Tim Liew, Alexei Kavokin, and Yuri Rubo deserve very special acknowledgements. Antonio Quattropani and Paolo Schwendiman have constantly helped with many discussions and their indefectible support of theorist/experimentalist collaborations. Last, but not least, this work would not have been possible without the very high-quality samples prepared by François Morier-Genoud and Fauzia Jabeen. The work has been carried out within the framework of the Quantum Photonics National Center of Competence in research financed by the Swiss National Science Foundation under project N° 153620. It has also been financed by ERC

under the Polaritronics Advanced Grant contract N° 291120. Complementary funding for conferences and meetings has been obtained through the Latsis Foundation and the Polatom network of the European Science Foundation.

## References

[1] C. Weisbuch, N. Nishioka, A. Ishikawa, Y. Arakawa, Observation of the coupled exciton–photon mode splitting in a semiconductor quantum microcavity, Phys. Rev. Lett. 69 (1992) 3314–3317.
[2] B. Deveaud-Plédran, On the condensation of polaritons, J. Opt. Soc. Am. B, Opt. Phys. 29 (2012) A138–A145.
[3] B. Deveaud, Exciton–polariton Bose condensates, Annu. Rev. Condens. Matter Phys. 6 (2015) 155–176.
[4] T. Byrnes, Na Young Kim, Y. Yamamoto, Exciton–polariton condensates, Nat. Phys. 10 (2014) 803–813.
[5] J. Kasprzak, M. Richard, S. Kundermann, A. Baas, P. Jeambrun, J. Keeling, F.M. Marchetti, M.H. Szymańska, R. André, J.L. Staehli, V. Savona, P.B. Littlewood, B. Deveaud Le Si Dang, Bose–Einstein condensation of exciton polaritons, Nature 443 (2006) 409.
[6] R. Balili, V. Hartwell, D. Snoke, L. Pfeiffer, K. West, Bose–Einstein condensation of microcavity polaritons in a trap, Science 316 (2007) 1007.
[7] S. Christopoulos, G. Baldassarri Höger von Högersthal, A.J.D. Grundy, P.G. Lagoudakis, A.V. Kavokin, J.J. Baumberg, G. Christmann, R. Butté, E. Feltin, J.-F. Carlin, N. Grandjean, Room-temperature polariton lasing in semiconductor microcavities, Phys. Rev. Lett. 98 (2007) 126405.
[8] J.D. Plumhof, T. Stoferle, L. Mai, U. Scherf, R.F. Mahrt, Room-temperature Bose–Einstein condensation of cavity exciton–polaritons in a polymer, Nat. Mater. 13 (2014) 247.
[9] K.S. Daskalakis, S.A. Maier, R. Murray, S. Kena-Cohen, Nonlinear interactions in an organic polariton condensate, Nat. Mater. 13 (2014) 272.
[10] A. Amo, D. Sanvitto, F.P. Laussi, D. Ballarini, E. del Valle, M.D. Martin, A. Lemaître, J. Bloch, D.N. Krizhanovskii, M.S. Skolnick, C. Tejedor, L. Viña, Collective fluid dynamics of a polariton condensate in a semiconductor microcavity, Nature 457 (2009) 291–295.
[11] A. Amo, J. Lefrère, S. Pigeon, C. Adrados, C. Ciuti, I. Carusotto, R. Houdré, E. Giacobino, A. Bramati, Superfluidity of polaritons in semiconductor microcavities, Nat. Phys. 5 (2009) 805.
[12] G. Nardin, G. Grosso, Y. Leger, B. Pietka, F. Morier-Genoud, Benoit Deveaud-Plédran, Quantum turbulence in a polariton fluid, Nat. Phys. 7 (2011) 635.
[13] A. Amo, S. Pigeon, D. Sanvitto, V.G. Sala, R. Hivet, I. Carusotto, F. Pisanello, G. Lemenager, R. Houdre, E. Giacobino, C. Ciuti, A. Bramati, Polariton superfluids reveal quantum hydrodynamical solitons, Science 332 (2011) 1167.
[14] G. Grosso, G. Nardin, Y. Léger, F. Morier-Genoud, B. Deveaud-Plédran, Soliton instabilities and vortex streets formation in a polariton quantum fluid, Phys. Rev. Lett. 107 (2011) 245301.
[15] R. Hivet, H. Flayac, D.D. Solnyskhov, D. Tanese, T. Boulier, D. Andreoli, J. Bloch, E. Giacobino, A. Kavokin, A. Bramati, G. Malpuech, A. Amo, Half-solitons in a polariton quantum fluid behave like magnetic monopoles, Nat. Phys. 8 (2012) 724–728.
[16] V. Kohnle, Y. Léger, M. Wouters, M. Richard, M.T. Portela-Oberli, B. Deveaud-Plédran, From single particle to superfluid excitations in a polariton gas, Phys. Rev. Lett. 106 (2011) 255302.
[17] V. Kohnle, Y. Leger, M. Wouters, M. Richard, M.T. Portella-Oberli, B. Deveaud, Four-wave mixing excitations in a dissipative polariton quantum fluid, Phys. Rev. B 86 (2012) 064508.
[18] A. Baas, J.P. Karr, M. Romanelli, A. Bramati, E. Giacobino, Optical bistability in semiconductor microcavities in the nondegenerate parametric oscillation regime: analogy with the optical parametric oscillator, Phys. Rev. B 70 (2004) 161307.
[19] D. Bajoni, E. Semenova, A. Lemaitre, S. Bouchoule, E. Wertz, P. Senellart, S. Barbay, R. Kuszelewicz, J. Bloch, Optical bistability in a GaAs-based polariton diode, Phys. Rev. Lett. 101 (2008) 266402.
[20] T.C.H. Liew, A.V. Kavokin, I.A. Shelykh, Optical circuits based on polariton neurons in semiconductor microcavities, Phys. Rev. Lett. 101 (2008) 016402.
[21] A. Amo, T.C.H. Liew, C. Adrados, R. Houdre, E. Giacobino, A.V. Kavokin, A. Bramati, Exciton–polariton spin switches, Nat. Photonics 4 (2010) 361.
[22] Y.G. Rubo, Half vortices in exciton polariton condensates, Phys. Rev. Lett. 99 (2007) 106401.
[23] K. Lagoudakis, T. Ostatnick, A.V. Kavokin, Y.G. Rubo, R. André, B. Deveaud-Plédran, Observation of half-quantum vortices in an exciton–polariton condensate, Science 326 (2009) 974–977.
[24] A.V. Kavokin, G. Malpuech, M.M. Glazov, Optical spin Hall effect, Phys. Rev. Lett. 95 (2005) 136601.
[25] C. Leyder, M. Romanelli, J.Ph. Karr, E. Giacobino, T.C.H. Liew, M.M. Glazov, A.V. Kavokin, G. Malpuech, G.A. Bramati, Observation of the optical spin Hall effect, Nat. Photonics 3 (2007) 628.
[26] M. Wouters, Resonant polariton–polariton scattering in semiconductor microcavities, Phys. Rev. B 76 (2007) 045319.
[27] N. Takemura, S. Trebaol, M. Wouters, M.T. Portella-Oberli, B. Deveaud, Polaritonic Feshbach resonance, Nat. Phys. 10 (2014) 500.
[28] N.A. Gippius, I.A. Shelykh, I.D.D. Solnyshkov, S.S. Gavrilov, Y.G. Rubo, A.V. Kavokin, S.G. Tikhodeev, G. Malpuech, Polarization multistability of cavity polaritons, Phys. Rev. Lett. 98 (2007) 236401.
[29] T.K. Paraïso, M. Wouters, Y. Léger, F. Morier-Genoud, B. Deveaud-Plédran, Multistability of a coherent spin ensemble in a semiconductor microcavity, Nat. Mater. 9 (2010) 655.
[30] F. Koyama, S. Kinoshita, K. Iga, Room-temperature continuous wave characteristics of a GaAs vertical cavity surface emitting laser, Appl. Phys. Lett. 55 (1989) 221.
[31] C.J. Chang-Hasnain, J.P. Harbison, G. Hasnain, A.C. Von Lehmen, L.T. Florez, N.G. Stiffel, Dynamic polarization and transverse mode characteristics of vertical cavity surface emitting lasers, IEEE J. Quantum Electron. 27 (1991) 1402.
[32] R. Houdré, R.P. Stanley, U. Oesterle, M. Ilegems, C. Weisbuch, Room-temperature cavity polaritons in a semiconductor microcavity, Phys. Rev. B 49 (1994) 16761.
[33] S. Pau, G. Björk, J. Jacobson, H. Cao, Y. Yamamoto, Microcavity exciton–polariton splitting in the linear regime, Phys. Rev. B 51 (1995) 14437.
[34] R. Houdré, C. Weisbuch, R.P. Stanley, U. Oesterle, P. Pellandini, M. Ilegems, Measurement of cavity-polariton dispersion curve from angle-resolved photoluminescence experiments, Phys. Rev. Lett. 73 (1994) 2043.
[35] S. Dufferwiel, F. Fras, A. Trichet, P.M. Walker, F. Li, L. Giriunas, M.N. Makhonin, L.R. Wilson, J.M. Smith, E. Clarke, M.S. Skolnick, D.N. Krizhanovskii, Strong exciton–photon coupling in open semiconductor microcavities, Appl. Phys. Lett. 104 (2014) 192107.
[36] Benjamin Besga, Cyril Vaneph, Jakob Reichel, Jérôme Estève, Andreas Reinhard, Javier Miguel-Sánchez, Ataç Imamoğlu, Thomas Volz, Polariton boxes in a tunable fiber cavity, Phys. Rev. Appl. 3 (2015) 014008.
[37] L. Tinkler, P.M. Walker, E. Clarke, D.N. Krizhanovskii, F. Bastiman, M. Durska, M.S. Skolnick, Design and characterization of high optical quality InGaAs/GaAs/AlGaAs-based polariton microcavities, Appl. Phys. Lett. 106 (2015) 021109.
[38] C. Ouellet-Plamondon, G. Sallen, F. Jabeen, D.Y. Oberli, B. Deveaud, Multiple polariton modes originating from the coupling of quantum wells in planar microcavity, Phys. Rev. B 92 (2015) 075313.
[39] P. Cilibrizzi, A. Askitopoulos, M. Silva, F. Bastiman, E. Clarke, J.M. Zajac, W. Langbein, P.G. Lagoudakis, Polariton condensation in a strain-compensated planar microcavity with InGaAs quantum wells, Appl. Phys. Lett. 105 (2014) 191118.
[40] N.Y. Kim, et al., Dynamical d-wave condensation of exciton–polaritons in a two-dimensional square-lattice potential, Nat. Phys. 7 (2011) 681–686.
[41] J.P. Reithmaier, M. Röhner, H. Zull, F. Schäfer, A. Forchel, P.A. Knipp, T.L. Reinecke, Size dependence of confined optical modes in photonic quantum dots, Phys. Rev. Lett. 78 (1997) 378.

[42] See for example: H.S. Nguyen, D. Gerace, I. Carusotto, D. Sanvitto, E. Galopin, A. Lemaître, I. Sagnes, J. Bloch, A. Amo, Acoustic black hole in a stationary hydrodynamic flow of microcavity polaritons, Phys. Rev. Lett. 114 (2015) 036402.
[43] G. Nardin, Phase resolved imaging of exciton polaritons, PhD thesis, 2011, EPFL N°5002.
[44] O. El Daïf, A. Baas, J.-P. Brantut, R. Idrissi Kaitouni, J.L. Staehli, F. Morier-Genoud, B. Deveaud, T. Guillet, Polariton quantum boxes in semiconductor microcavities, Appl. Phys. Lett. 88 (2006) 061105.
[45] R. Idrissi Kaitouni, O. El Daïf, M. Richard, P. Lugan, A. Baas, F. Morier-Genoud, J.D. Ganière, J.L. Staehli, T. Guillet, V. Savona, B. Deveaud, Engineering the spatial confinement of exciton–polaritons in semiconductors, Phys. Rev. B 74 (2006) 155311.
[46] L. Dominici, D. Colas, S. Donati, J.P. Restrepo Cuartas, M. De Giorgi, D. Ballarini, G. Guirales, J.C. López Carreño, A. Bramati, G. Gigli, E. del Valle, F.P. Laussy, D. Sanvitto, Ultrafast control and Rabi oscillations of polaritons, Phys. Rev. Lett. 113 (2014) 226401.
[47] W. Langbein, B. Patton, Heterodyne spectral interferometry for multidimensional nonlinear spectroscopy of individual quantum systems, Opt. Lett. 31 (2006) 1151–1153.
[48] J. Kasprzak, S. Reitzenstein, E.A. Muljarov, C. Kistner, C. Schneider, M. Strauss, S. Höfling, A. Forchel, W. Langbein, Up on the Jaynes–Cummings ladder of a quantum-dot/microcavity system, Nat. Mater. 9 (2010) 304–308.
[49] Naotomo Takemura, On the physics of polariton interactions, PhD thesis EPFL N°XXX, 2015.
[50] H. Abbaspour, G. Sallen, S. Trebaol, F. Morier-Genoud, M.T. Portella-Oberli, B. Deveaud, The effect of a noisy driving field on a bistable polariton system, Phys. Rev. B 92 (2015) 165303.
[51] Taofiq Paraiso, Dynamics of interactions of confined microcavity polaritons, PhD thesis, EPFL N° 4726, 2010.
[52] M. Vladimirova, S. Cronenberger, D. Scalbert, K.V. Kavokin, A. Miard, A. Lemaître, J. Bloch, D. Solnyshkov, G. Malpuech, A.V. Kavokin, Polariton–polariton interaction constants in microcavities, Phys. Rev. B 82 (2010) 075301.
[53] N. Takemura, S. Trebaol, M. Wouters, M.T. Portella-Oberli, B. Deveaud, Heterodyne spectroscopy of polariton spinor interactions, Phys. Rev. B 90 (2014) 195307.
[54] M. Combescot, M. Dupertuis, O. Betbeder-Matibet, Polariton–polariton scattering: exact results through a novel approach, Europhys. Lett. 79 (2007) 17001.
[55] M. Vladimirova, S. Cronenberger, D. Scalbert, K.V. Kavokin, A. Miard, A. Lemaître, J. Bloch, D. Solnyshkov, G. Malpuech, A.V. Kavokin, Polariton–polariton interaction constants in microcavities, Phys. Rev. B 82 (2010) 075301.
[56] N. Takemura, S. Trebaol, M.D. Anderson, S. Biswas, D.Y. Oberli, M.T. Portella-Oberli, B. Deveaud, Dephasing effects on coherent exciton–polaritons and the breaking of the strong coupling regime, Phys. Rev. B 92 (2015) 235305.
[57] N. Takemura, S. Trebaol, M. Wouters, M.T. Portella-Oberli, B. Deveaud, Heterodyne spectroscopy of polariton spinor interactions, Phys. Rev. B 90 (2014) 195307.
[58] M. Wouters, Resonant polariton–polariton scattering in semiconductor microcavities, Phys. Rev. B 76 (2007) 045319.
[59] A.L. Ivanov, M. Hasuo, N. Nagasawa, H. Haug, Two-photon generation of excitonic molecules in CuCl: an exactly solvable bipolariton model and high-precision experiments, Phys. Rev. B 52 (1995) 11017.
[60] E. Hanamura, Giant two-photon absorption due to excitonic molecule, Solid State Commun. 12 (1973) 951.
[61] I. Carusotto, T. Volz, A. Imamoglu, Feshbach blockade: single-photon nonlinear optics using resonantly enhanced cavity polariton scattering from biexciton states, Europhys. Lett. 90 (2010) 37001.
[62] C. Ciuti, V. Savona, C. Piermarocchi, A. Quattropani, P. Schwendimann, Role of the exchange of carriers in elastic exciton–exciton scattering in quantum wells, Phys. Rev. B 58 (1998) 7926.
[63] V. Axt, K. Victor, T. Kuhn, The exciton–exciton continuum and its contribution to four-wave mixing signal, Phys. Status Solidi, B 206 (1998) 189.
[64] T. Ostreich, K. Schönhammer, L.J. Sham, Exciton–exciton correlation in the nonlinear optical regime, Phys. Rev. Lett. 74 (1995) 4698.
[65] N.H. Kwong, R. Takayama, I. Rumyantsev, M. Kuwata-Gonokami, R. Binder, Evidence of nonperturbative continuum correlations in two-dimensional exciton systems in semiconductor microcavities, Phys. Rev. Lett. 87 (2001) 027402.
[66] R. Takayama, N. Kwong, I. Rumyantsev, M. Kuwata-Gonokami, R. Binder, T-matrix analysis of biexcitonic correlations in the nonlinear optical response of semiconductor quantum wells, Eur. Phys. J. B 25 (2002) 445.
[67] C. Ciuti, P. Schwendimann, B. Deveaud, A. Quattropani, Theory of the angle-resonant polariton amplifier, Phys. Rev. B 62 (2000) R4825.
[68] T. Lecomte, D. Taj, A. Lemaitre, J. Bloch, C. Delalande, J. Tignon, P. Roussignol, Polariton–polariton interaction potentials determination by pump-probe degenerate scattering in a multiple microcavity, Phys. Rev. B 89 (2014) 155308.
[69] S. Inouye, M.R. Andrews, J. Stenger, H.-J. Miesner, D.M. Stamper-Kurn, W. Ketterle, Observation of Feshbach resonances in a Bose–Einstein condensate, Nature 392 (6672) (1998) 151–154.
[70] E.A. Donley, N.R. Claussen, S.L. Cornish, J.L. Roberts, E.A. Cornell, C.E. Wieman, Dynamics of collapsing and exploding Bose–Einstein condensates, Nature 412 (6844) (2001) 295–299.
[71] M. Greiner, C.A. Regal, D.S. Jin, Emergence of a molecular Bose–Einstein condensate from a Fermi gas, Nature 426 (6966) (2003) 537–540.
[72] M. Theis, G. Thalhammer, K. Winkler, M. Hellwig, G. Ruff, R. Grimm, J. Hecker Denschlag, Tuning the scattering length with an optically induced Feshbach resonance, Phys. Rev. Lett. 93 (2004) 123001.
[73] M. Wouters, Resonant polariton–polariton scattering in semiconductor microcavities, Phys. Rev. B 76 (2007) 045319.
[74] A.L. Ivanov, M. Hasuo, N. Nagasawa, H. Haug, Two-photon generation of excitonic molecules in CuCl: an exactly solvable bipolariton model and high-precision experiments, Phys. Rev. B 52 (1995) 11017–11033.
[75] M. Vladimirova, et al., Polarization controlled nonlinear transmission of light through semiconductor microcavities, Phys. Rev. B 79 (2009) 115325.
[76] M.M. Glazov, et al., Polariton–polariton scattering in microcavities: a microscopic theory, Phys. Rev. B 80 (2009) 155306.
[77] J.I. Inoue, et al., Renormalized bosonic interaction of excitons, Phys. Rev. B 61 (2000) 045316.
[78] N.H. Kwong, et al., Third-order exciton–correlation and nonlinear cavity-polariton effects in semiconductor microcavities, Phys. Rev. B 64 (2001) 045316.
[79] M. Saba, F. Quochi, C. Ciuti, U. Oesterle, J.L. Staehli, B. Deveaud, G. Bongiovanni, A. Mura, Crossover from exciton to biexciton polaritons in semiconductor microcavities, Phys. Rev. Lett. 85 (2000) 385–388.